



¹. I. I. AHMED, ². T. YAHAYA, ³. J. A. ADEBISI, ⁴. N. I. AREMU, ⁵. A.G.F. ALABI, ⁶. S.B. LYON

STRESS CORROSION CRACKING OF AUSTENITIC STAINLESS STEELS IN POTENTIOSTATICALLY CONTROLLED CHLORIDE ENVIRONMENTS AT AMBIENT TEMPERATURE

^{1,6}. Materials Performance Centre, University of Manchester, Manchester, M13 9PL, UNITED KINGDOM

²⁻⁴. Department of Materials and Metallurgical Engineering, University of Ilorin, Ilorin, NIGERIA

⁵. Department of Materials Science Engineering, Kwara State University, Malete, NIGERIA

Abstract: In the earlier study carried out to assess the effect of applied potentials on stress corrosion cracking of Austenitic Stainless Steels (ASS), Type 304L in a potentiostatically controlled chloride environment at ambient temperature, the assessment of cracks in failed specimen was limited to optical microscope. In this present study, Scanning Electron Microscope (SEM) was used in addition to optical microscope to gain a better understanding of the Stress Corrosion Cracking (SCC) mechanism in the failed specimen. Stress corrosion cracking tests were carried out on annealed ASS using a Slow Strain Rate Test (SSRT) technique in sodium chloride solution acidified with hydrochloric acid at ambient temperature. Post-mortem assessments of failed specimens were carried out using both optical and SEM. The study showed that plastic elongation, ultimate tensile strength and time to failure decrease as the applied potential increases during the slow strain rate test. The study showed that immunity of ASS to chloride SCC was improved when the electrochemical potential was maintained in the primary passive potential range. Post-mortem assessment of failed specimens showed evidences of SCC and ductile failure on the fracture surface. The cross sectional analysis of the failed samples showed cracks that were predominantly transgranular stress corrosion cracks.

Keywords: Failure; Passive film; Stress corrosion crack; Stainless Steels; SEM

1. INTRODUCTION

The performance of Austenitic Stainless Steels (ASS) is considered satisfactory due to their good combination of high strength, ductility and general corrosion resistance even at elevated temperature (Couvant et al., 2005, Garda, 2000). They are widely used in process plants, cryogenic plants, food industry and nuclear industry (Arioka et al., 2007). However, austenitic stainless steels are susceptible to localised corrosion failure including pitting corrosion, crevice corrosion and stress corrosion cracking (Lai et al., 2009, Garcia et al., 2002).

In furtherance to earlier study (Ahmed et al., 2015) on the above subject matter, where the assessment of cracks propagation in the failed specimens was limited to use of optical microscope, the present study has delved deeper on the assessment with the incorporation of preliminary potentiodynamic polarisation scan data and use of scanning electron microscope for better understanding of the dominant failure mechanism.

2. EXPERIMENTAL PROCEDURE. MATERIALS & METHODS

The material used was the same austenitic stainless steels, Type 304L used earlier. The chemical composition of the steels is shown in Table 1. The ASS plate (300 × 100 × 30mm) as received was initially solution annealed at 1050°C for 30 minutes and quenched in water. Fast cooling was done to prevent intergranular precipitation of the chromium carbide by sensitisation process described elsewhere (Garcia et al., 2002, Kain et al., 2004). The material was subsequently heat treated at 400°C and furnace cooled to partially relieve internal stresses and to remove any martensite which may have formed due to fast cooling (Ahmed et al., 2013b). The average grain size and the 0.2% offset yield strength of the annealed material were 68µm and 290MPa respectively.

Table 1: Chemical Composition (wt%) of Alloying Elements

C	Cr	Mn	N	Ni	P	S	Si
0.030	18.387	1.804	0.086	8.133	0.034	0.005	0.411

≡ Preliminary Potentio-dynamic polarisation Measurement

The preliminary potentiodynamic polarisation scan carried out to ascertain the range of applied potentials required for the SCC test. The test carried out on three orthogonal planes (longitudinal, L, Transverse, T and Short-transverse, S) of 20% cold rolled samples

from the same material to be used for SCC test. The test was carried out in an electrolyte solution containing 1M sodium chloride acidified to the pH of 1.5 with hydrochloric acid. The Working Electrode was connected through a stainless steel wire spot welded to the test sample. The Auxiliary Electrode (AE) made of platinum wire was connected as the cathode in the electrolytic cell. The Saturated Calomel Electrode was used as the Reference Electrode (RE). The potentiodynamic polarisation measurement was carried out at Scan Rate of 0.1667mV/s in aerated and ambient Temperature Conditions.

≡ **Slow Strain Rate Test in Potentio-statically Controlled Chloride Environment**

The slow strain rate test was carried out on 100kN Instron 5500R equipped with Bluehill software for test and result analysis. The tensile specimens used were machined from the centre of the plates along the prior longitudinal directions. A schematic diagram of the tensile specimen and its dimensions are shown in Figure 1. Typical sample name used include ANL which represents annealed sample made from longitudinal direction. Preliminary sample preparation included wet grinding and polishing with increasingly fine silicon carbide paper in order of 400, 600, 800 and 1200 grit sizes to remove machining grooves. The sample was then degreased with acetone and later rinsed with deionised water. The sample surface area to be exposed to electrolyte was measured for subsequent calculation of corrosion current density, while other area was insulated from the environment with wax.

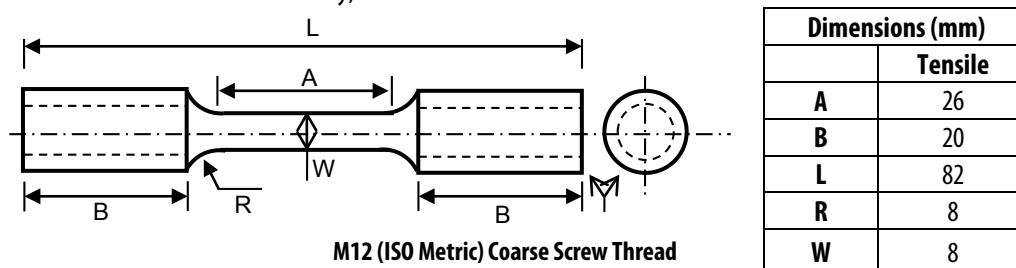


Figure 1: Schematic Diagram of the Slow Strain Rate Test Specimen and Dimension

The stress corrosion cracking susceptibility test in a chloride environment was carried out using slow strain rate method. The test was carried out in a solution containing 1M sodium chloride acidified to the pH of 1.5 with hydrochloric acid. The volume of custom made SCC cell used for the test was 250ml (approximately 40ml/cm² of the exposed gauge length area). The chloride environment was potentiostatically controlled with the aid of an ACM instruments Research Potentiostat. The Working Electrode was connected through a stainless steel wire spot welded to the test sample. The Auxiliary Electrode (AE) was connected to cathode made from 1m Platinum wire wound round a plastic cylinder placed within the SCC cell. The Saturated Calomel Electrode was used as the Reference Electrode (RE). The test was carried out at the cross-head speed 6.3×10^{-6} mm/s which is equivalent to the strain rate of 2.4×10^{-7} s⁻¹ in line with the ASTM standard(2000). The corrosion current was measured with the aid of a Pico Higher Resolution Data Logger connected with the potentiostat and test rig computer. The SCC tests were carried out at three different potentials namely: -125mV, -100mV and -50mV with respect to the SCE, to assess the SCC susceptibility of the material in the different corrosion environments. The chloride environment was potentiostatically controlled with the aid of an ACM instruments Research Potentiostat, and the tests were all carried out at ambient temperature and in aerated open environment.

≡ **Post-Mortem Optical Microscopy**

The post-mortem optical microscopy was carried out on failed samples using an Olympus light microscope installed with AxioVision (Release 4.7.2) digital camera and application software. The gauge length surface area of failed samples was observed to determine the extent of cracks after the stress corrosion cracking test. The images of cracks and corrosion pit were observed on the samples and processed with the application software. The image obtained from optical micrographs was used as a guide for the sectioning of samples across the cracks. The samples were subsequently sectioned for scanning electron microscopy.

≡ **Post-Mortem Scanning Electron Microscopy**

Zeiss EVO 60 scanning electron microscope was used for examination of failed samples fracture surfaces. After fractographic examination, samples were subsequently sectioned across crack, ground and polished with Oxide Polishing Suspension (colloidal silica suspension), OPS for metallographic examination. This was done to examine the crack propagation mode. The scanning electron microscopy was carried out using the secondary electrons and Accelerating Voltage of 20 kV.

3. RESULTS AND DISCUSSION

≡ **Preliminary Potentio-dynamic polarisation Measurement Result**

The results of preliminary test carried out on three orthogonal planes of 20% cold rolled samples are shown in Figure 2. Preliminary polarisation scan was necessary to inform the choice of range of applied potentials needed for the SCC test. The polarisation scan was carried out on deformed sample which was only available rather than annealed material used in SCC test. This is not expected to affect the objective of the study on the basis of earlier studies (Mazza et al., 1979, Fu et al., 2009) which have shown that primary

passivation is not significantly affected by deformation degrees. Hence, the choice of three potentials (-125mV, -100mV and -50mV) investigated in the SCC test, was made from the preliminary Potentiodynamic polarisation measurement. Two of the applied potentials (-100mV and -50mV) fall within the metastable pitting potential region, while -125mV corresponds to the passive potential that allows the material to maintain a protective corrosion resistance passive film.

The test at applied potential of -125mV was done to assess the SCC susceptibility of the material at passive potential condition, considering the fact that SSRT is so severe to force material to fail. The potential in metastable pitting regions was to facilitate the initiation of SCC at the root of the corrosion pits.

It was also observed from Figure 2 that, the applied potential was not affected by the test sample direction, while the corrosion current density showed an obvious difference. The highest corrosion current density occurred on the longitudinal plane (L) and least corrosion current density occurred on the short-transverse plane (S) (see Figure 2). The possible suggestion for the observed difference can be attributed to grain boundaries density on the respective planes of deformed sample.

≡ Effect of Applied Potentials on Stress Corrosion Cracking Susceptibility

The results of stress corrosion cracking tests are shown in Figure 3. The plots of applied stress against engineering strain and the plot of current density against time to failure are shown in Figure 3A & B respectively. The detailed results of tests are contained in Table 2. The effect of applied potential was quite obvious from the Plastic elongation (ductility), the Ultimate Tensile Strength (UTS) and from Time to Failure (TTF).

The ductility and ultimate tensile strength of material decrease as the applied potential increases. Similarly, time to failure also decreases as applied potential increases. The decrease in the time to failure and mechanical properties of the material may be attributed to significant increase in the corrosion rate caused by increase in the applied potential. The plots of corrosion current density against time to failure in Figure 3B showed that corrosion current density increases as applied potential increases. The increased corrosion current density with time to failure was attributed to crevice corrosion between the elongated sample and the SCC cell. The plot of corrosion current density against time to failure also showed that first current peak coincided with onset of plastic elongation. The curve showed a repeated pattern of sudden increase in corrosion current density followed by gradual decay with time, which is characteristic of stress corrosion cracking failure.

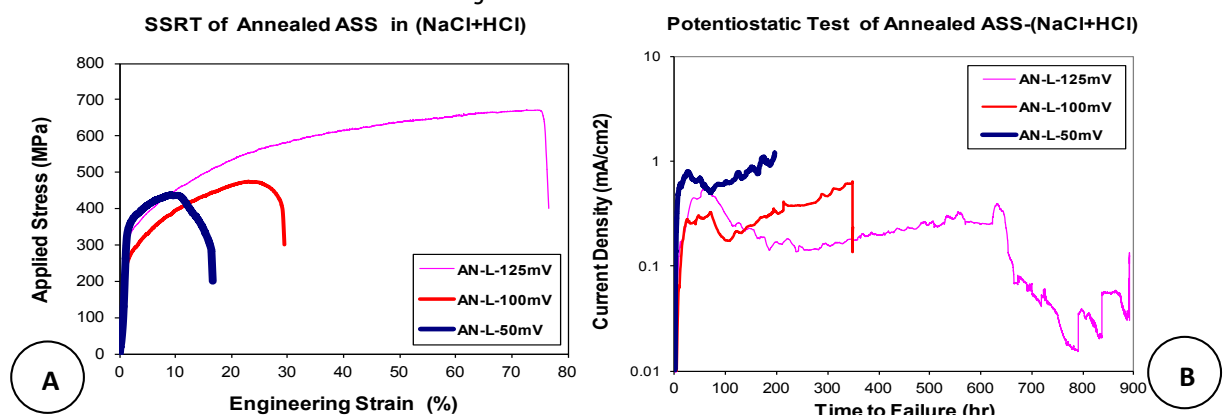


Figure 3: SSRT Curves for Annealed Samples Tested at Strain Rate of $2.4 \times 10^{-7} \text{ s}^{-1}$, pH of 1.5, and Applied Potentials of -125mV, -100mV and -50mV at Ambient Temperature: Applied Stress Vs Strain (A) and Current Density Vs Time to Failure (B)

The test at applied potential of -125mV took 891 hours before failure occurred. This was obviously too long, while failure occurred too quickly at 197 hours when the applied potential was increased to -50mV (see Figure 2) due to accelerated corrosion process. The applied potential of -125mV represents the passive potential where corrosion process was expected to be at minimal level. Hence, the SCC test was largely dominated by mechanical process.

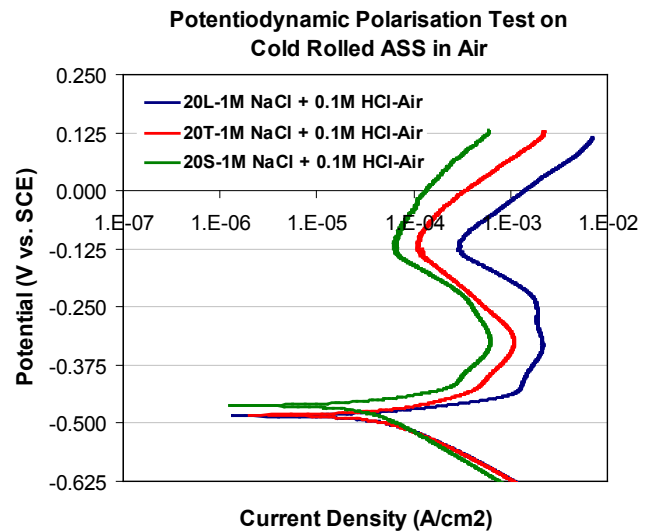


Figure 2: Potentiodynamic Polarisation Measurement on 20% Cold Rolled ASS, Type 304L, in Solution containing 1M Sodium Chloride + 0.1M Hydrochloric Acid at Scan Rate of 0.1667mV/s in Aerated and Ambient Temperature Conditions

Comparing and contrasting the effects of applied potential have shown that SCC susceptibility can be mitigated and held under control if electrochemical potential is maintained in the passive potential region. On the other hand, when applied potential of -100mV was used, failure time was considerably reduced at 348 hours. Therefore, tests at -100mV appeared to strike a balance between competing process dominated by corrosion and mechanical effects.

The plot of plastic elongation against applied potentials is shown in the Figure 4 and the detailed results of the samples tested at different applied potentials are shown in the Table 2. The significant increase in the corrosion rate may have been the reason for decrease in the plastic elongation as the applied potential increases (see Figure 4).

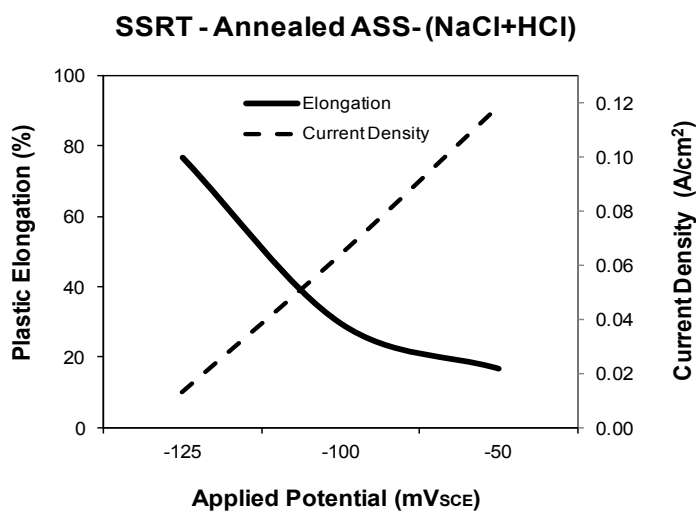


Figure 4: Effect of Applied Potentials on Plastic Elongation and Corrosion Current Density for Annealed Samples Tested in Chloride Environment at Strain Rate of $2.4 \times 10^{-7} \text{s}^{-1}$, pH of 1.5 at Ambient Temperature

Table 2: Summary Results of the SSRT (SCC) on Annealed Sample at Strain Rate of $2.4 \times 10^{-7} \text{s}^{-1}$ (Test Speed of $6.3 \times 10^{-6} \text{mm/s}$) and Ambient Temperature

Material Condition	Applied Potential (mV)	Yield Strength (MPa)	UTS (MPa)	Elongation (%)	Time to Failure (Hr)	Current Density A/cm ²
Annealed	-125	300	672	76.7	891	0.13
	-100	240	474	29.5	348	0.64
	-50	340	437	16.6	197	1.19

≡ Post-Mortem Optical Microscopy of the SCC Samples

The results of optical microscopy of annealed samples tested at different applied potentials are shown in the Figure 5. The three samples failed at a similar location, at the point of contact between the SCC cell and the sample. The failure at this location was probably facilitated by crevice corrosion between the cell and sample due to reduction in cross-sectional area as the sample elongated during the test. However, the cracks and corrosion pits shown in the Figure 5 were found on the gauge length area (see inset in Figure 5A). All three samples showed evidence of cracks perpendicular to the loading (longitudinal) direction.

The cracks on sample tested at applied potential -50mV are quite faint and thinner than other two samples (Figure 5C). This may have been caused by the lower plastic elongation due to accelerated corrosion process that dominated the test. In addition to the observed cracks on the samples tested at applied potential -50mV, corrosion pits of about 0.8mm diameter were also observed on the sample (see Figure 5D).

≡ Post-Mortem Scanning Electron Microscopy of Failed Samples

The scanning electron micrographs of annealed samples investigating effects of applied potential on the SCC are shown in Figure 6. The fracture surface and crack cross section of sample tested at applied potential of -125mV are shown in Figures 6A&B respectively. The fracture surface showed areas of SCC with evidence of secondary cracks along the loading direction and that of pure ductile failure. The area of ductile failure were characterised by dimples (see insets in Figure 6A). It was understood from SSRT results that the test at applied potential of -125mV was dominated by mechanical process because of very low strain rate used. This may have been the reason why secondary cracks observed were more conspicuous than in other samples tested at applied potentials of -100mV and -50mV.

The SEM micrograph of crack cross section in the gauge length area is shown in Figure 6B. The cross sectional view of the sample showed evidence of crack which appeared to be quite thin. The crack was expected to be more widely opened under load prior to the final failure. Complete removal of load after failure may have led to crack closure due to elastic recovery. The crack is suggested to be transgranular crack. The single crack propagated across the loading direction without obvious branch. Fracture surface and crack cross section of sample tested at applied potential of -100mV are shown in the Figure 6C & D respectively. Additional information from the fracture surface of sample tested at applied potential of -100mV was aggressive corrosion, which was not so obvious on sample tested at applied potential of -125mV. The cross section of the crack in the Figure 6D also showed a thin crack with branches. The cracks were transgranular in nature.

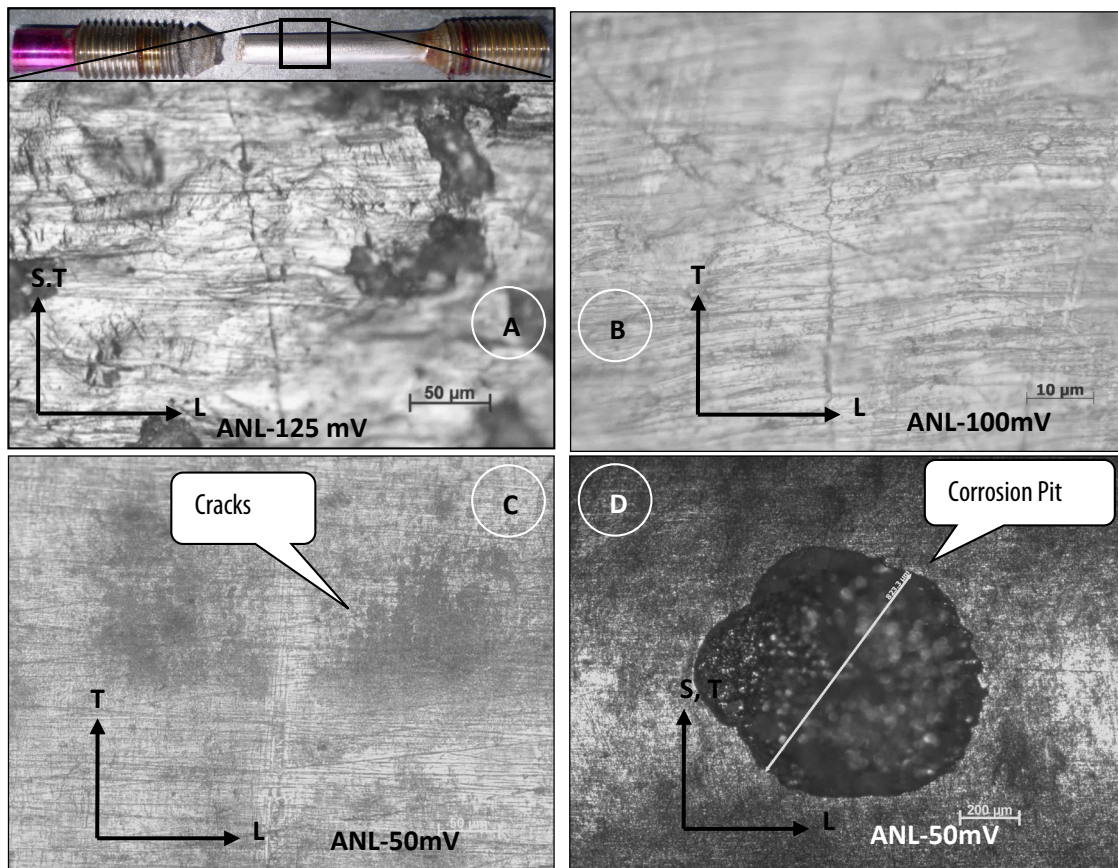


Figure 5: Optical Micrographs of Annealed Samples Tested at Strain Rate of $2.4 \times 10^{-7} \text{s}^{-1}$, pH of 1.5, and Applied Potentials of: -125mV (A), -100mV (B) and -50mV (C and D) at Ambient Temperature

The fracture surface of sample tested at applied potential of -50mV (Figure 6E) showed evidence of excessive corrosion (pitting and crevice) which dominated the process. The fracture surface also contained an area of SCC with secondary cracks and an area of ductile failure dominated by ductile dimples. The SEM micrographs of crack cross section are shown in the Figure 6F. The cracks were faint and quite thin, this may be attributed to higher corrosion rate and low mechanical process. The plastic elongation was relatively lower compared to the samples tested at the applied potential of -125mV and -100mV (see Figure 4). The inset in Figure 6F showed one of the corrosion pits and what appeared to be a crack at the root of the corrosion pit.

4. DISCUSSION

The Slow Strain Rate Tests have shown that, plastic elongation, ultimate tensile strength and time to failure decrease as the applied potential increases. The plastic elongation was significantly reduced when applied potential was increased from -125mV to -50mV (Figure 4). The decrease in the plastic elongation when applied potential was increased from -125mV to -50mV was attributed to the enhanced corrosion process caused by transpassive dissolution of primary passive film (Zheng and Bogaerts, 1993). The tests carried out at passive potential of -125mV demonstrated that SCC susceptibility can be arrested if test is maintained at primary passivation range. The immunity of ASS to chloride SCC was obviously improved when electrochemical potential was maintained at primary passive potential range. This improvement may be credited to the formation of stable chromium-rich passive film that continuously help to protect the substrate whenever crack or pit opens up (Burstein et al., 1993, Hashimoto et al., 1976).

Again, the rupture pattern of sample tested at applied potential of -100mV was outstanding (see Figure 4). The tangent on the curves just beyond the UTS showed evidence of gradual failure compared to samples tested at -125mV and -50mV. The test at -100mV signified the optimal condition for SCC test and represents the balance between competing effects of mechanical and corrosion factors. The applied potential must be such that it will not be too low so that failure is not dominated by mechanical process and must be too high, otherwise failure may be dominated by corrosion process. Samples tested at applied potential of -100mV seemed to represent the optimal condition as indicated by the rupture curve. This is an indication that material had sufficient time for crack propagation to actually occur before final fracture occurred. This is typical of SCC propagation where cracks grow through repeated process of film rupture by mechanical strain and repassivation of the protective chromium oxide film (Garcia et al., 2002, Sedriks, 1996).

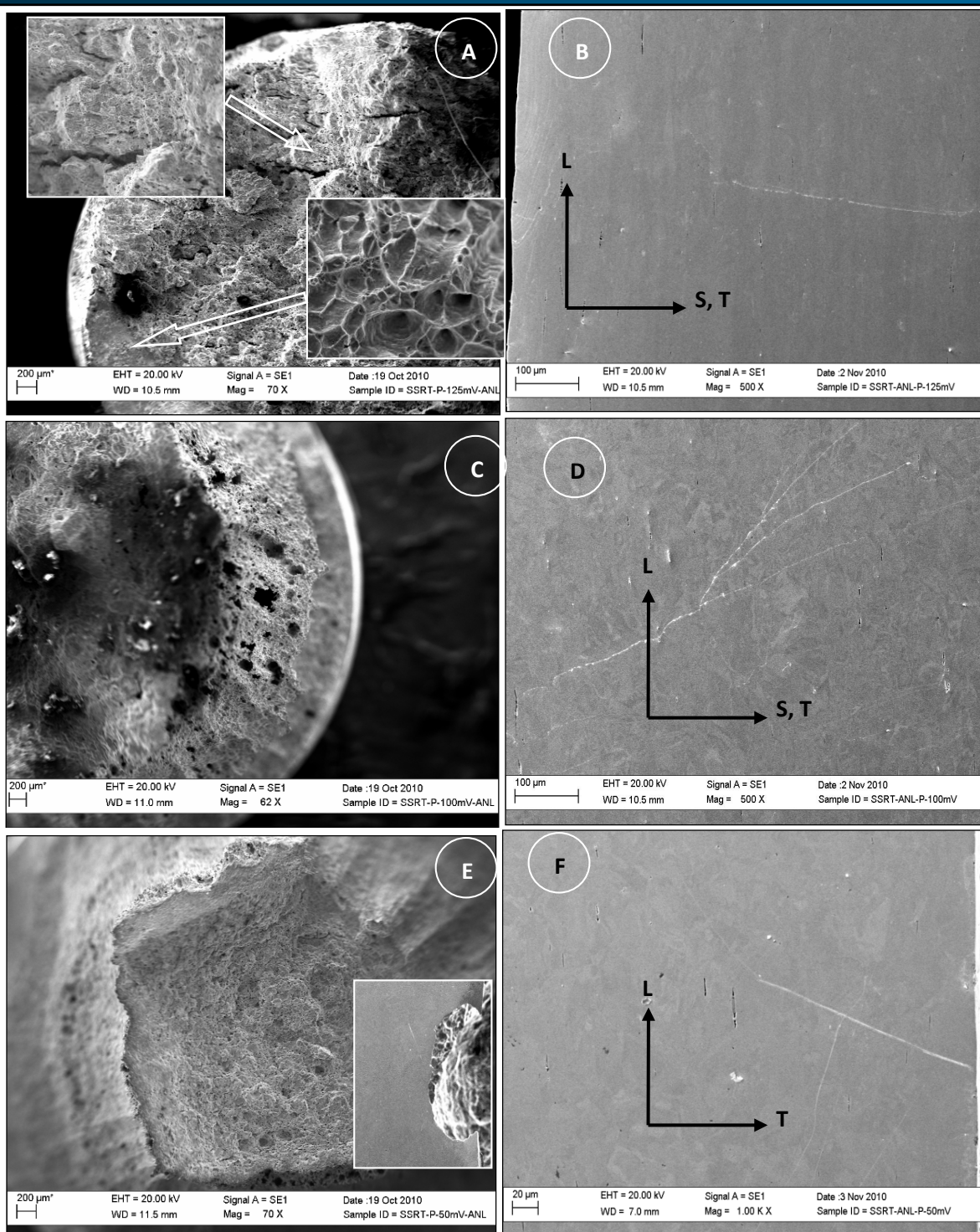


Figure 6: SEM Micrographs of Annealed Samples Tested at Strain Rate of $2.4 \times 10^{-7} s^{-1}$, pH of 1.5 and Ambient Temperature, at the Applied Potentials of: -125mV (A & B), -100mV (C & D) and -50mV (E & F), showing the Fracture Surface and Crack Cross Section, respectively.

The correlation of corrosion current density with time to failure showed a number of current spikes followed by gradual decay. The sudden increase in corrosion current density is attributed to break down of passive film and exposure of metallic substrate to the environment. The rapid corrosion of bared metal substrate was the reason for the sudden rise in the corrosion current density. The subsequent gradual decay in corrosion current density was largely attributed to self healing mechanism of stainless steels through repassivation of chromium-rich oxide film (Burstein et al., 1993, Garcia et al., 2002). It was also understood from the results that the first current peak consistently occurred at the location correlated to onset of plastic elongation. It appears as if the peak has occurred due to the temporary breaking of the interatomic bond when the yield point was exceeded. However, Burstein et al. (Burstein et al., 1993) proposed the first current peak represents the nucleation of metastable pit which eventually died before propagation.

The Post-mortem optical and scanning electron microscopy of the fractured samples showed that, fracture surface contained regions of ductile failure and stress corrosion cracking. Ductile region were characterised by ductile dimples whilst the SCC showed secondary cracks which propagated along the loading axis. The secondary cracks were suggested to have developed at austenite-ferrite interface due to the strain incompatibility and localised heterogeneous deformation between austenite and ferrite (Ahmed et al., 2013a). The cross sectional analysis of failed samples showed that cracks propagated perpendicular to loading axis and the crack observed were predominantly transgranular SCC.

5. CONCLUSIONS

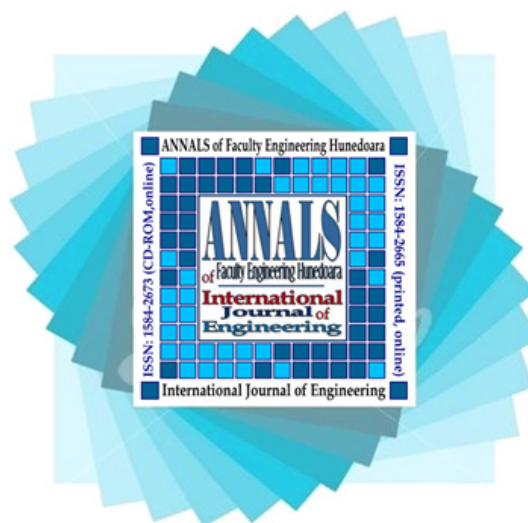
The following are conclusions at the end of study investigating the effect of applied potential on the SCC susceptibility of austenitic stainless steels, Type 304L:

1. The stress corrosion cracking studies showed that plastic elongation, ultimate tensile strength and time to failure decreased as the applied potential increases during the slow strain rate test.
2. The increase in corrosion current density with applied potential was attributed to increase in corrosion rate due to transpassive dissolution of primary passive film.
3. The immunity of ASS to chloride SCC was improved when electrochemical potential was maintained at primary passive potential range. The improvement was attributed to formation of stable chromium-rich passive film that continuously help to protect the substrate when crack opens up.
4. Post-mortem scanning electron microscopy of fractured samples following slow strain rate test in chloride environment showed that, the fracture surface contained SCC and ductile failure regions.
5. The SCC region contained secondary cracks which propagated along the loading axis and ductile regions characterised by dimples. The cross sectional analysis of failed samples showed that cracks propagated perpendicular to loading axis and cracks observed were predominantly transgranular SCC.

References

- [1.] ASTM Standard Practice for Slow Strain Rate Testing to Evaluate the Susceptibility of Metallic Materials to Environmentally Assisted Cracking, Designation: G 129-00, West Conshohocken, USA, ASTM International, 2000.
- [2.] Ahmed, I. I., Alabi, A. G. F., Odusote, J. K., Aremu, I. N., Adebisi, J. A., Yahaya, T., Talabi S. I., Yahya, R. A. & Lyon, S. B.: Stress Corrosion Cracking of Austenitic Stainless Steel in Chloride Environment, Nigerian Journal of Engineering, in press, 2015.
- [3.] Ahmed, I. I., Da Fonseca, J. Q. & Sherry, A. H.: Effect of strain paths and residual delta ferrite on the failure of cold rolled austenitic stainless steels, type 304L, The Journal of Strain Analysis for Engineering Design, 48 (7), 410-419, 2013a.
- [4.] Ahmed, I. I., Da Fonseca, J. Q. & Sherry, A. H.: Effects of martensite development on lattice strain evolution during the in situ deformation of austenitic stainless steels at cryogenic temperatures, The Journal of Strain Analysis for Engineering Design, 2013b.
- [5.] Arioka, K., Yamada, T., Terachi, T. & Chiba, G.: Cold Work and Temperature Dependence of Stress Corrosion Crack Growth of Austenitic Stainless Steels in Hydrogenated and Oxygenated High-Temperature Water, Corrosion, 63 (12), 1114-1123, 2007.
- [6.] Burstein, G. T., Pistorius, P. C. & Mattin, S. P.: The nucleation and growth of corrosion pits on stainless steel, Corrosion Science, 35 (1994), 57-62, 1993.
- [7.] Couvant, T., Legras, L., Vaillant, F., Boursier, J. M. & Rouillon, Y.: Effect of strain-hardening on stress corrosion cracking of aisi 304L stainless steel in PWR primary environment at 360°C. Proc.of the Twelfth Intl. Conf.on Environmental Degradation of Materials in Nuclear Power Systems-Water Reactors. 1069-1081, 2005.
- [8.] Fu, Y., Wu, X., Han, E. H., Ke, W., Yang, K. & Jiang, Z.: Effects of cold work and sensitization treatment on the corrosion resistance of high nitrogen stainless steel in chloride solutions, Electrochimica Acta, 54 (5), 1618-1629, 2009.
- [9.] Garcia, C., Martin, F., Tiedra, P. D., Alonso, S. & M. L. Aparicio: Stress Corrosion Cracking Behaviour of Cold-Worked and Sensitized Type 304 Stainless Steels using the Slow Strain Rate Test, NACE, 58, 2002.
- [10.] Garda, C.: Effect of prior cold work on intergranular and transgranular corrosion in type 304 stainless steels: Quantitative discrimination by image analysis, Corrosion, 56 (3), 243-255, 2000.
- [11.] Hashimoto, K., Osada, K., Masumoto, T. & Shimodaira, S.: Characteristics of passivity of extremely corrosion-resistant amorphous iron alloys, Corrosion Science, 16 (2), 71-76, 1976.
- [12.] Kain, V., Chandra, K., Adhe, K. N. & De, P. K.: Effect of cold work on low-temperature sensitization behaviour of austenitic stainless steels, Journal of Nuclear Materials, 334 (2-3), 115-132, 2004.
- [13.] Lai, C. L., Tsay, L. W., Kai, W. & Chen, C.: Notched tensile tests of cold-rolled 304L stainless steel in 40 wt.% 80 °C MgCl₂ solution Corrosion Science, 51 (2), 380-386, 2009.

- [14.] Mazza, B., Pedferri, P., Sinigaglia, D., Cigada, A., Fumagalli, G. & Re, G.: Electrochemical and corrosion behaviour of work-hardened commercial austenitic stainless steels in acid solutions, *Corrosion Science*, 19 (7), 907-921, 1979.
- [15.] Sedriks, A. J.: *Corrosion of Stainless Steels*, New York, John Wiley & Sons, Inc., 1996.
- [16.] Zheng, J. H. & Bogaerts, W. F.: Effects of cold work on stress corrosion cracking of type 316L stainless steel in hot lithium hydroxide solution, *Corrosion*, 49 (7), 585-593, 1993.



ANNALS of Faculty Engineering Hunedoara – International Journal of Engineering



copyright © UNIVERSITY POLITEHNICA TIMISOARA, FACULTY OF ENGINEERING HUNEDOARA,
5, REVOLUTIEI, 331128, HUNEDOARA, ROMANIA
<http://annals.fih.upt.ro>